Effects of Multifunctional Cross-linkers on Rheology and Adhesion of Soft Nanostructured Materials

Xavier Callies, C. Véchambre, C. Fonteneau, F. Herbst, J.-M. Chenal, S. Pensec, Laurent Chazeau, W H Binder, Laurent Bouteiller, Costantino Creton

Effects of Multifunctional Cross-linkers on Rheology and Adhesion of Soft Nanostructured Materials

X. Callies[a,b†], C. Véchambre[d], C. Fonteneau[c], F. Herbst[e], J-M. Chenal[d], S. Pensec[c], L. Chazeau[d] , W. H. Binder[e], L. Bouteiller[c], and C. Creton[a,b*]*

[a]*Laboratoire de Sciences et Ingénierie de la Matière Molle, CNRS, ESPCI Paris, PSL Research University, 10 Rue Vauquelin, 75005 Paris, France*

[b]*Laboratoire Sciences et Ingénierie de la Matière Molle, Université Pierre et Marie Curie, Sorbonne-Universités, 10 rue Vauquelin, France*

[c]*Sorbonne Universités, UPMC Univ Paris 06, CNRS, IPCM, Chimie des Polymères, F-75005 Paris, France*

[d]*Laboratoire MATEIS, CNRS, INSA Lyon, 7 avenue Jean Capelle, Villeurbanne, 69100, France*

[e]*Chair of Macromolecular Chemistry, Institute of Chemistry, Faculty of Natural Science II (Chemistry, Physics and Mathematics), Martin Luther University Halle-Wittenberg, Halle 06120, Germany*

[†]*current address:* IPREM CNRS-UMR 5254, Equipe de Physique et Chimie des Polymères, Université de Pau et des Pays de l'Adour, Hélioparc, 2 avenue Président Angot, 64053 Pau Cedex 9, France

xavier.callies@univ-pau.fr, costantino.creton@espci.fr

Abstract

We investigate the nanostructure, the rheology and the adhesion of soft supramolecular materials elaborated by blending monofunctional and multifunctional poly(isobutene) (PIB) chains. Monofunctional PIB chains (PIBUT) are linear and unentangled polymer chains (M_n≈3kg/mol) functionalized in the middle by a bis-urea interacting moiety, able to self-associate by four hydrogen bonds. Covalent coupling of monofunctional PIB allows us to synthesize longer chains bearing two or three interacting moieties. These chains are then added to monofunctional PIB to prepare blends containing up to 10% of multifunctional PIB (M-PIBUT). The influence of M-PIBUT on the supramolecular nanostructure, which results from the self-assembly of stickers, is studied by Atomic Force Microscopy and Small Angle X-ray Scattering at room temperature. Multifunctional and monofunctional chains are shown to interact with each other to form bundles of rod-like aggregates. The consequences of these interactions on the rheology of the blends were studied by shear tests in the linear and non linear regimes, below and above the order-disorder transition temperature. A pronounced strengthening effect of M-PIBUT is observed at room temperature: the

supramolecular blends become more elastic and are more resistant to creep with increasing concentration of M-PIBUT. The effects of M-PIBUT on the nanostructure and the rheology suggest that M-PIBUT, which can link with more than one supramolecular aggregate, plays the role of a physical cross-linker. The impact of these supramolecular cross-linkers on the adhesion of the blends is studied by probe-tack tests and discussed by analyzing the in-situ deformation through the debonding images.

Introduction

The use of supramolecular chemistry within the field of polymers constitutes a well-known and inexhaustible toolbox for scientists to elaborate bioinspired, smart and high-tech materials[1]. The polymer chains in supramolecular materials are functionalized by strongly interacting moieties (sometimes called stickers). The reversible association between stickers (typically via hydrogen or metal-ligand bonds) induces the self-assembly of polymer chains and usually a well-defined and dynamic nanostructure[2]. Among the numerous studies focusing on the properties of these new materials, many of them reported the impact of the stickers on their rheology and revealed the contribution of several molecular mechanisms[3], such as the association/dissociation dynamics of dimers, the formation of clusters and phase segregation process[4,5,6,7]. The mechanical behavior of supramolecular materials is thus complex and investigations on model systems are required to design supramolecular polymer chains for specific applications.

Most past studies have focused on systems containing more than one sticker group per chain, which are likely to form reversible but rather elastic networks. For applications where having significant dissipative properties may be more important such as vibration damping or viscoelastic pressure-sensitive-adhesives, functionalizing the polymer chains with interacting moieties while keeping a high mobility of the chains remains a key-issue[8]. Along those lines, some of us have focused in the past on self-assembly and adhesive properties of short polyisobutylene chains (called PIBUT, M_n=3kg/mol) bearing a single sticker per chain located in its middle. In solution, these chains self-associate into cylindrical structures[9] while in the melt state, they form highly dynamic structures showing some long range order[10] below 68°C. The unique dissipative properties[10] of PIBUT gives an interesting and unexplored route for the elaboration of soft adhesives[11]. However, the liquid-like behavior of PIBUT at large deformation prevents a clean removal from the surface, which is an expected feature for soft adhesives. Inspired from recent studies in the field of hydrogels[12,13,14], our strategy to strengthen the nanostructure under strain and trigger some strain hardening at large strain consists in introducing multifunctional polymer chains as supramolecular cross-linkers.

The interactions between multifunctional and monofunctional chains are expected to physically cross-link the supramolecular aggregates and to finely tune the strain hardening in the melt state that would stabilize adhesive fibrils and possibly allow a clean removal of an

adhesive material. Multifunctional poly(isobutene) chains were then synthesized and mixed with PIBUT up to a weight concentration of 10%. The nanostructure of these blends was investigated by Atomic Force Microscopy and Small Angle X-ray Scattering while rheology was studied by oscillatory shear tests in the linear and non linear regimes. The adhesion of these model systems was explored by probe-tack tests and the effect of the rheological differences on the debonding mechanisms is then discussed by an insightful analysis of the debonding images[15].

Since the first investigations on soft materials in the 1960s, it is well known that their adhesive properties are closely linked to their rheology, in particular their viscoelasticity[16], strain-softening and strain-hardening mechanisms[17]. In numerous studies[18], the peeling and tack properties were correlated with the mechanical behavior of adhesives in linear and non-linear rheology. Although a wide range of model systems, from liquids[19,20,21] to solids[22,23], have been investigated, studies on supramolecular unentangled materials[24] have shown unusual adhesive properties, unpredicted by classical theories[18] developed for entangled and lightly crosslinked systems. In addition to designing high-tech and smart materials, supramolecular chemistry can be used to build new and well-defined materials with unusual properties. In line with the recent work on center-functionalized supramolecular poly(butylacrylate)[24], our present work underlines the complex role played by the non-linear rheology in controlling the adhesive properties of novel adhesive materials tested with classical debonding tests, such as the probe-tack test.

Experimental Section

Materials & Synthesis

The one pot-synthesis of PIBUT was previously described by Pensec and coworkers[9]. Briefly, 2,4-toluenediisocyanate (TDI) (98% from Aldrich) is coupled with two mono-amine end-functionalized poly(isobutene) chains provided by BASF (*Kerocom PIBA*). After purification by precipitation in ethyl acetate, the polymers were characterized by NMR spectroscopy and Size Exclusion Chromatography (SEC). The number average molecular weight is close to 3000g/mol and the dispersity is close to 1.3.

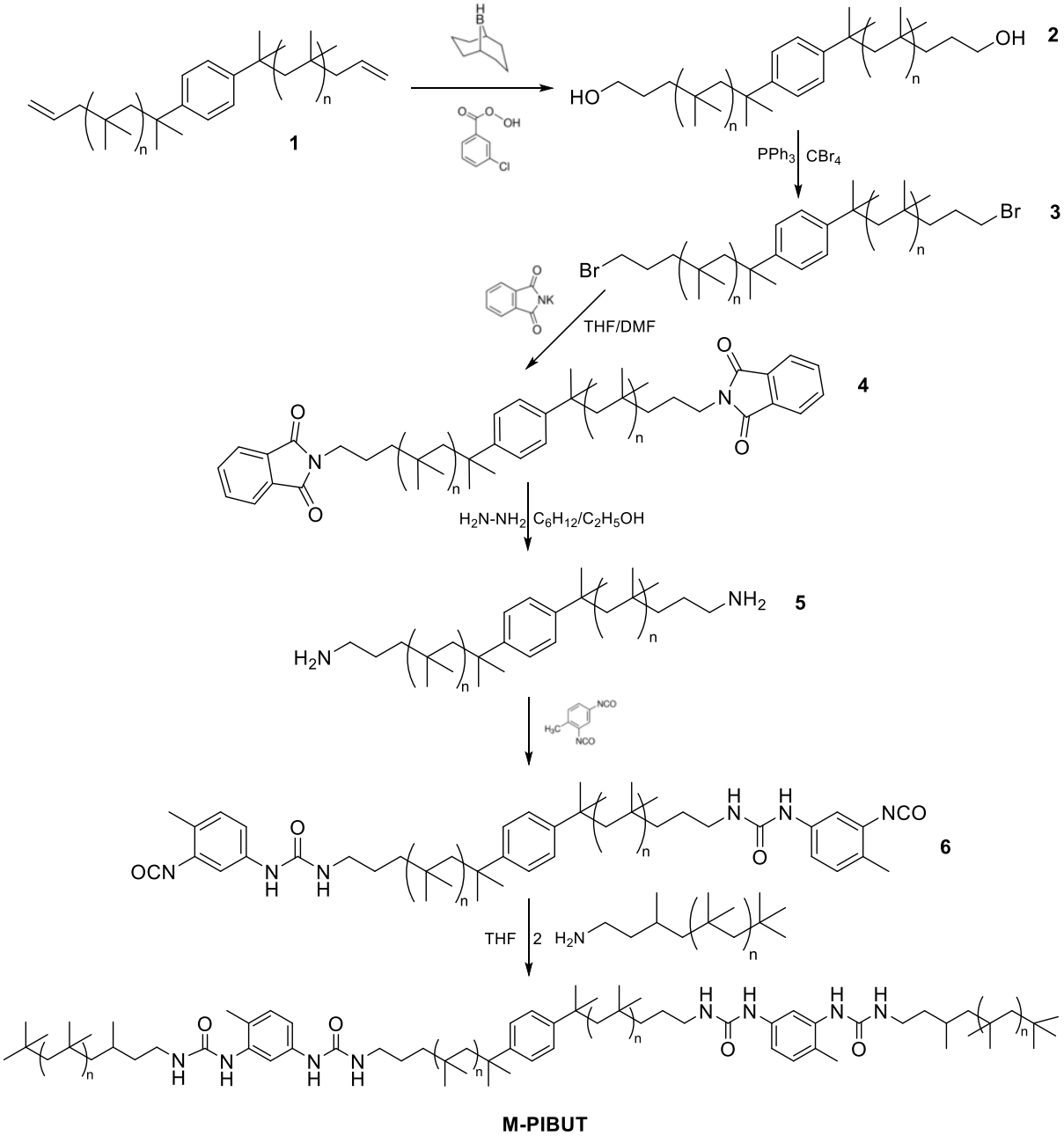

Figure 1: Synthesis scheme of multifunctional poly(isobutene) M-PIBUT.

For the multifunctional poly(isobutene), an amino telechelic poly(isobutene) (product **5** in figure 1) is synthesized first. The synthesis of **5** is carried out in four steps from a telechelic allyl poly(isobutene) (Mn = 9990 g/mol, Đ = 1.25) from Kaneka (see SI), according to previous literature[25]. As shown in figure 1, the synthesis of M-PIBUT is carried out in two steps from **5**. First telechelic isocyanate-bifunctionalized poly(isobutene) is obtained by reacting a slight excess of TDI with telechelic amine-bifunctionalized poly(isobutene) (**5**). In the second step, the remaining isocyanate groups react with amino-functionalized poly(isobutene) (NH_2-PIB) to give bis-urea moieties. Because of the statistical reaction between TDI and **5**, a mixture of products is actually obtained.

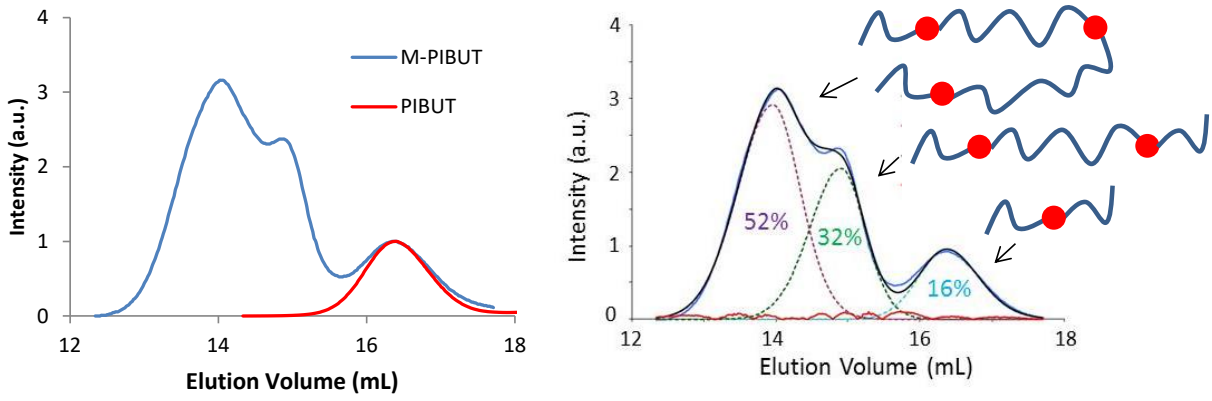

Figure 2: Comparison between SEC chromatograms of PIBUT and M-PIBUT (left) and analysis of the experimental chromatogram of M-PIBUT (right) as the sum of three peaks (see dashed lines). These peaks are interpreted as the contribution of the three main components of M-PIBUT: poly(isobutene) with either one, two or three bis-urea stickers per chain. The red curve is the difference between the sum of these peaks (the black line) and the experimental curve (the blue line).

After purification by precipitation, M-PIBUT was analyzed by SEC and NMR. As shown in figure 2, three different structures are clearly detected in the chromatogram of M-PIBUT (see SI for the fitting procedure). According to the reaction scheme, these three polymers are PIB chains containing respectively one, two or three bis-urea stickers. The decomposition of the experimental SEC chromatogram into three peaks allows to estimate the weight% of these three polymers: 16% for PIBUT, 32% for bi-functionalized PIB and 52% for tri-functionalized PIB. Finally PIBUT/M-PIBUT blends were prepared by dissolving both materials in toluene in suitable proportions. The solution was then deposited on a glass slide, left for 2 days at room temperature, and then for 2 more days at 70°C under vacuum to remove the solvent by evaporation.

Rheology

Linear viscoelastic measurements were performed on a stress-controlled rheometer DHR 3 (TA Instruments). The frequency dependence of the viscoelastic moduli *G'* and *G''* was characterized with a parallel plate geometry (diameter 25 mm) at 25°C and 80°C. The

rheometer was equipped with a Peltier device and an insulating thermal cover to regulate the temperature of the sample from 0 to 80°C. Samples were annealed for 2 hours between the two plates at constant temperature before measurements.

Samples	PIBUT (w%)	M-PIBUT (w%)	Sticker Density (w%)
PIBUT	100	0	7.8
Blend_0.1	99.9	0.1	7.7
Blend_0.5	99.5	0.5	7.6
Blend_1	99	1	7.5
Blend_5	95	5	6.6
Blend_10	90	10	5.8

Table 2: Composition of the supramolecular blends.

Adhesion tests

Adhesion tests were carried out on thin (100 µm ± 10µm) adhesive layers deposited on glass slides (2.6*10*0.2 cm^3, purchased from Preciver) by slow evaporation. Solutions were prepared by dissolving 300mg of supramolecular material in 2mL of toluene. Solutions were then deposited on glass slides, left for 2 days under a glass cover at room temperature, and then for 2 more days at 70°C under reduced pressure (~200mbar) to remove the residual solvent. The dry films thickness was measured by a white light scanning technique with an optical profilometer (Microsurf 3D, Fogale nanotech).

The home-made probe-tack set-up is described in detail elsewhere[26,24]. The probe-tack test[27] as we carried it out, consists in bringing the surface of a solid probe into contact with the thin adhesive layer coated on a rigid substrate and in measuring the force F_T required to detach it at a constant debonding speed V_{deb}. During the debonding step, the displacement *d(t)* of the probe relative to the adhesive layer is measured in order to calculate the thickness of the adhesive layer *h(t)*:

$$h(t) = d(t) - K^* F_T(t) + h_0 \quad (1)$$

with h_0 the initial thickness of the adhesive film and $K=5.5\ \mu m./N$ the compliance of the apparatus (measured with a blank test). Probe-tack curves conventionally plot the nominal stress $\sigma_0(t)=F_T(t)/A_0$ versus the nominal strain $\varepsilon_0(t)=(h(t)-h_0)/h_0$ or the stretching ratio $\lambda_0(t)=1+\varepsilon_0(t)$, where A_0 is the contact area between the probe and the adhesive layer at the maximum compression stage. The area under the $\sigma_0=f(\varepsilon_0)$ curve is used to calculate the debonding energy of the soft layer, W_{adh} (J/m^2), i.e. the energy necessary to detach the probe from the layer for the given traction speed:

$$W_{adh} = h_0 \int \sigma_0 \, d\varepsilon_0 \quad (2)$$

The experimental procedure of the alignment between the probe and the glass slide was recently described in detail[24]. In order to get a perfectly smooth and reflective surface, the stainless steel probes (diameter Φ=5.95 ± 0.02mm) were mechanically polished.

In our home-made set-up[26], the thin adhesive layer in contact with the probe is observed via an optical microscope connected to a CCD camera. The force and the displacement data are synchronized with the video captures of the test via an outside timer. In the case of the formation of a fibrillar structure during the debonding process, images can be analyzed by using the methods developed by Tanguy and coworkers[15] in order to characterize the *in-situ* elongation of the material during the debonding step of the probe-tack test. This method was previously explained in detail[24].

Briefly, a true stress σ_e, i.e. the component of the stress parallel to the tensile direction, in the walls between cavities before the equilibration of pressure as well as in the remaining fibrils after the equilibration of pressure, can be estimated:

$$\sigma_e = \frac{F_m}{A_e} \quad (3)$$

with the force F_m required to stretch fibrils and the load-bearing area A_e, i.e. the projected area of fibrils. In the presence of bubbles, F_m is calculated by subtracting the force F_p due to the work against the atmospheric pressure from the measured force F_T. The force $F_p \approx A_c P_{atm}$ is estimated by considering the projected area A_c of a convex envelop around bubbles and the atmospheric pressure $P_{atm} \approx 10^5$Pa. After the coalescence of all bubbles, F_p=0. In the case of viscoelastic fluids, the elongational flow in the fibrils can be characterized by an approximate local transient elongational viscosity η^+ in the fibril walls via the Hencky strain rate $\dot{\epsilon}_H$:

$$\eta^+ = \frac{\sigma_e}{\dot{\epsilon}_H} \quad (4)$$

The Hencky strain rate $\dot{\epsilon}_H$ is calculated by considering an effective elongation $< \lambda >$ along the tensile direction in the thinnest cross-section of the walls by assuming a deformation of the wall at constant volume.

$$\dot{\epsilon}_H = \frac{d(ln<\lambda>)}{dt} \quad \text{with } <\lambda> = \frac{A_0}{A_e} \quad (5)$$

Atomic Force Microscopy

The experimental set-up was previously described elsewhere[28]. Briefly, AFM experiments were performed with a Di3100 AFM apparatus connected to a Nanoscope V scanning probe controller (VEECO Instruments, Plainview, NY). All images were obtained at ambient temperature in tapping mode using silicon cantilevers (SSS-NCH tips from Nanosensor) with a nominal spring constant of 42 $N \cdot m^{-1}$ and a high resonance frequency of 330 kHz. The average scanning speed was less than 20 $\mu m \cdot s^{-1}$. The sample was diluted in toluene, a droplet was then placed on a hard surface (indifferently a mica or a silica wafer) and the solvent was slowly evaporated overnight; then the sample was submitted to a partial vacuum during a week to allow complete solvent evaporation. The vertical z resolution was about 0.5 nm, while the x−y resolution was about 5 nm or less. For all samples, at least three different areas were analyzed to ensure image repeatability. Height images (not shown) indicate a flat surface with a maximum difference in height of 5 nm for a square image of 1 µm. The observations were found to be the same on silica or mica wafer substrates. Moreover, given the sample thickness which is above 100 µm, i.e., much larger than the characteristic length of the microstructure discussed in this manuscript, one can reasonably conclude that the AFM observations are independent of the substrate and would not be modified by a modification of its surface chemistry.

X-ray Scattering

Small angle X-ray scattering (SAXS) experiments were carried out on X-ray apparatus equipped with a copper rotating anode (λ=1.54 Å) (Rigaku Corporation, Japan), a Gobel's mirrors collimation system (Elexience, France).). The two-dimensional (2D) patterns were recorded by a CCD Camera (Princeton Instrument). The distance between sample and detector was set at 400 mm. The exposure time was set at 5 min. Thus, scattered intensity was plotted as a function of the scattering vector q (equal to $(4\pi/\lambda) \sin \theta$) from the integration of the scattered intensity over the azimuthal angle, from 0 to 360°. Each pattern was corrected from the background scattering. All samples were first diluted in toluene and deposited on a thin kapton film; the solvent was slowly evaporated overnight and the sample was then placed in partial vacuum during a week. Since no attempt was made to ensure a fixed mass of the samples, absolute intensity comparisons of the patterns for different samples is not quantitative. For all patterns the kapton signal was subtracted.

Results

Nanostructure

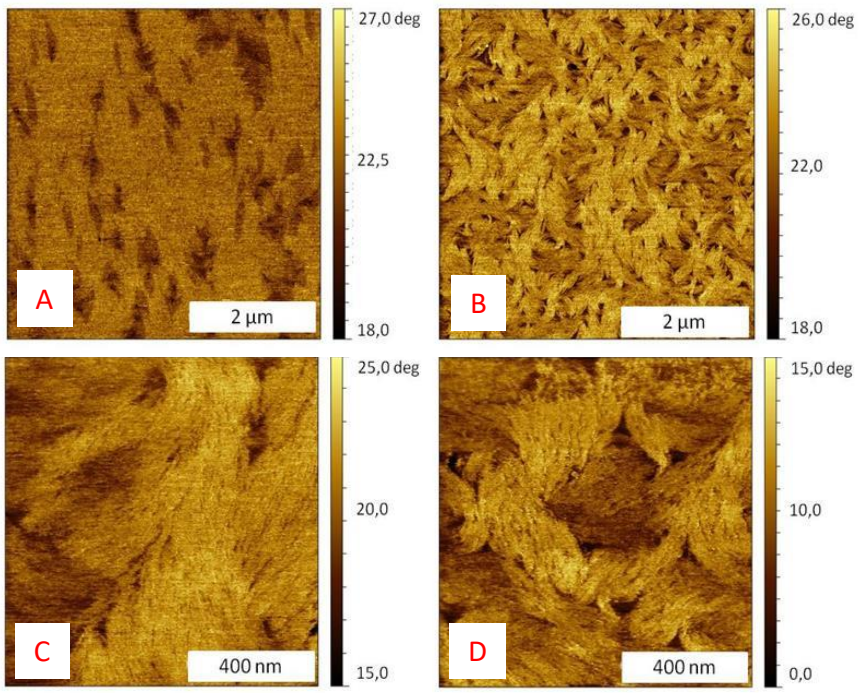

Figure 3: Phase Image by AFM for PIBUT (A), Blend_1 (B & C) and Blend_10 (D)

First the molecular organization in PIBUT/M-PIBUT blends was studied by AFM. As shown in figure 3, the chemical composition has a strong influence on the morphology observed at the surface. Despite some small darker areas, the preponderant white zone observed in image 3.A reveals that the surface of PIBUT is homogenous at a micrometric scale. In the blend containing M-PIBUT, small anisotropic objects are observed with a random orientation at the surface (see fig 3.B). As clearly shown in picture 3.C and 3.D, these objects are formed by the assembly of filaments parallel to each other.

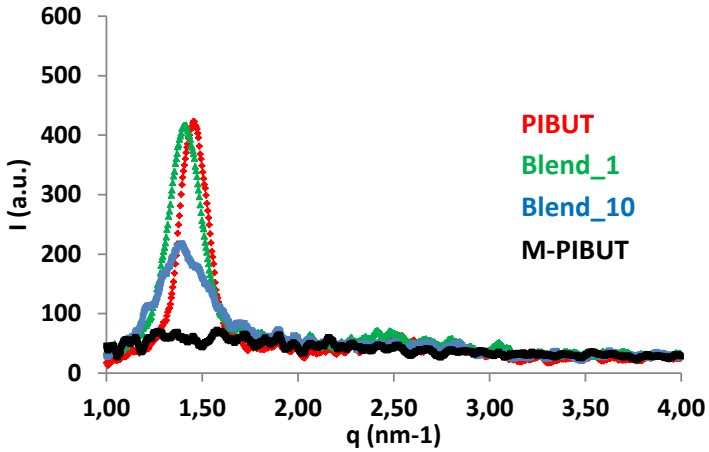

Figure 4: Variation of the scattered intensity I (a.u.) with the scattering vector q in SAXS experiments for PIBUT, M-PIBUT and their respective blends at 1 and 10% of M-PIBUT.

The variation in nanostructure induced by the addition of multi-functionalized chains was also studied by SAXS. In figure 4, the variation of the scattered intensity with the scattering vector q is characterized by one peak for PIBUT and the M-PIBUT/PIBUT blends. This scattering peak shifts towards lower q values and becomes broader when the concentration of multi-functionalized chains increases. For pure M-PIBUT, no peak is detected.

Two conclusions can be drawn from the AFM and SAXS experiments. First the investigation of the nanostructure of the supramolecular blends by SAXS highlights the interactions of M-PIBUT with PIBUT and more specifically, the incorporation of multifunctional chains into rod-like aggregates (observed by AFM). As shown in previous studies[28], the X-ray peak characterizes the quality (width of the peak) and characteristic distance (position of the peak) of the alignment of supramolecular rod-like filaments induced by the self-assembly of bis-urea moieties. The average characteristic distance measured at d≈4.3nm for pure PIBUT increases up to d≈4.6nm for 10% of M-PIBUT. In pure PIBUT, the distance between the comb-shaped filaments is linked to the length of the PIB side chains (1500g/mol)[28]. In the chemical structure of M-PIBUT, the spacer between stickers (10000g/mol) is longer than twice the side chains of PIBUT (see scheme in figure 2). The expansion of the supramolecular structure, which results from the addition of M-PIBUT, could be due to the difference in size of the PIB strands between monofunctional and multifunctional chains.

While the addition of M-PIBUT modifies little the supramolecular structure at small scale, the broadening of the scattering peak reveals more disorder over a larger length scale induced by the incorporation of multifunctional chains at higher concentrations (10%). This is consistent with the detection of randomly oriented bundles observed at the surface of the blends by AFM. This effect on the long range order between filaments is linked to the intimate mixing between both components at the nanometer length scale. Based on the rheological data shown in the next section, a strong kinetic effect is proposed to explain the effect of the multifunctional chains on nanostructure in the discussion part.

Rheology

The influence of the multi-functionalized PIB on the linear rheology of the blends is studied by comparing the rheological behavior of the different blends at room temperature and 80°C. At high temperature, all materials are viscoelastic fluids (see figure 5); a flow part is clearly observed at low ω (G"≫G' and G" ~ ω) while a viscoelastic zone (G''≈G') is identified at higher frequencies. Yet, viscoelastic moduli vary little over the investigated concentration range: G" is only twice higher for Blend_10 than for PIBUT at low frequency. It is worth noting that blends and PIBUT are not Newtonian fluids, since no plateau is clearly observed at low frequency for the complex viscosity $\eta^*=\sqrt{((G')^2+(G'')^2)}/\omega$ and G' tends to be parallel to G'' at very low frequencies (see figure S6 in SI). Such behavior was previously observed for supramolecular polymers functionalized in the middle by strong stickers[29].

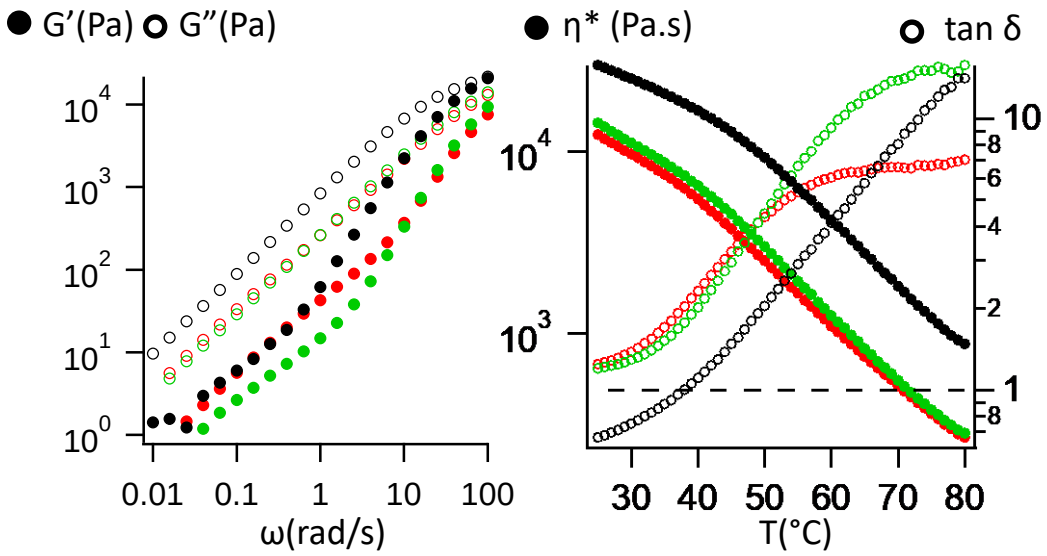

Figure 5: Frequency dependence of G' and G'' (Pa) at 80°C (left) and variation of the complex viscosity η*(Pa.s) and that of the damping factor tan(δ) with temperature at a fixed angular frequency ω=1rad/s at small deformation for PIBUT (red markers), Blend_1 (green) and Blend_10 (black).

As previously reported by Courtois and coworkers[10], the rheological behavior of PIBUT at room temperature is sensitive to the thermal and mechanical history of the sample. Such sensitivity was also observed for the blends. In order to obtain reproducible results, samples were annealed at 80°C for 1 hour and the temperature was then reduced in a controlled way (1°C/min). After annealing the sample at T=25°C in the rheometer for 24 hours, the rheological behavior was finally characterized by shear tests in the linear regime.

The variation of the complex viscosity η^* and that of the damping factor $tan(\delta)=G"/G'$ during the temperature ramp is shown at a fixed angular frequency ω=1rad/s in the linear regime for PIBUT and blends in figure 5. As expected, η^* increases and $tan(\delta)$ decreases as the temperature decreases. It is worth noting that the elastic part of the rheological response is

more pronounced for the supramolecular blends than for pure PIBUT when T is decreasing. For low temperatures (T≤50°C), *η** increases and *tan(δ)* decreases when [M-PIBUT] increases . While a dissipative behavior is still observed for PIBUT and Blend_1 at the end of the temperature ramp (i.e. *tan(δ)*≥1), Blend_10 is characterized by a more elastic character (i.e. *tan(δ)* ≤1).

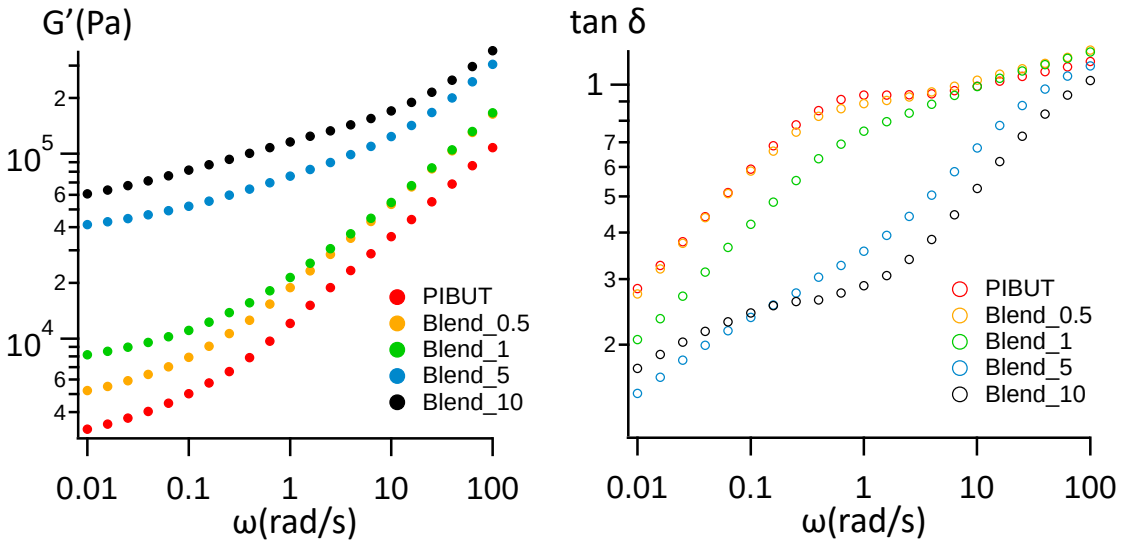

Figure 6: Frequency dependence of G' (Pa) and tan δ (Pa) at 25°C for PIBUT and the supramolecular blends. The viscoelastic moduli were measured 24 hours after the cooling ramp was applied.

After the temperature ramp, samples were annealed at 25°C for 24 hours. During the annealing time, the viscoelastic moduli vary with time (see figure S7). The time dependence is particularly pronounced at low frequency (ω<1rad/s): G' increases and tan(δ) decreases with increasing annealing time. As discussed in previous studies[10,28], the increasingly elastic character of the supramolecular materials with annealing time reveals the slow kinetics of supramolecular self-assembly as well as the slow organization of rod-like aggregates into bundles. Similar supramolecular dynamics was expected for PIBUT and the blends, since all materials have the same stickers and the same polymer matrix. After an annealing time t=24h at 25°C, all materials behave as a soft dissipative solids, characterized by an elastic plateau at low frequency and a dissipative response at high frequency (tanδ≈1) (see figure 6). However a significant increase of the elastic plateau with the concentration of multifunctional chains is observed, from G'= 3kPa (PIBUT) to G'= 60kPa (Blend_10).

The strain dependence of the viscoelastic moduli was also characterized at low and high frequency (ω=6.28rad/s and ω=6.28 10^{-2} rad/s) and data are shown for PIBUT, Blend_0.5 and Blend_1 in figure 7. At higher concentrations, interfacial slip prevents a characterization of the rheological properties at very large strain in such a geometry. A typical response of a yield stress fluid is observed for all materials at both frequencies. At large deformations, the decrease of the viscoelastic moduli with increasing γ reveals a softening mechanism and, for

all tests except for Blend_1 at ω=6.28 10^{-2} rad/s, a liquid-like response (G">G') is observed beyond a critical deformation γ_c.

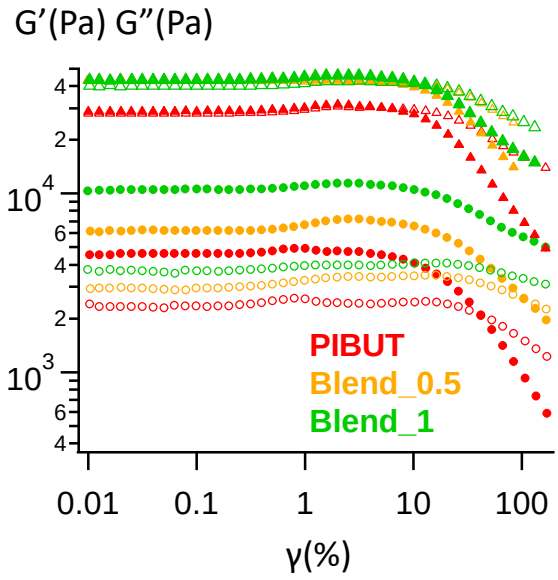

Figure 7: Strain dependence of G' (filled markers) and G" (unfilled markers) at 25°C at ω=6.28rad/s (triangles) and ω=6.28.10^{-2} rad/s (circles) for PIBUT, Blend_0.5 and Blend_1.

Similar responses are observed for the three materials at high ω while the dependence on the concentration [M-PIBUT] is more pronounced at low frequency. For ω=2π. 10^{-2} rad/s, G' and G" intersect at γ_0=40% for PIBUT and γ_0=130% for Blend_0.5 while G' remains higher than G" for Blend_1. The discrepancy between both investigated frequencies highlights the impact of the polymer matrices that relax at short time scales[29], and that of the supramolecular self-assembly that relaxes at much longer time scales, as further detailed in the discussion part.

As discussed in the latter part, the effects of multifunctional chains on the rheology of supramolecular blends are those expected for physical or chemical cross-linkers according to the theory of rubber elasticity: increasing the concentration of M-PIBUT induces a more elastic behavior at small deformations and a stronger cohesion at large deformations. The consequences of these rheological changes on the adhesive properties are investigated in the following part.

Adhesion

Representative stress-strain curves are shown for probe-tack tests carried out at room temperature at V_{deb}=100 µm/s and V_{deb}=1µm/s in figure 8. A semi-log representation was chosen to highlight the variations of the shapes of the stress-strain curves when [M-PIBUT] increases from 0 to 5%.

For the faster speed, V_{deb}=100 µm/s, corresponding to average initial strain rates ~ 1 s^{-1}, over the [M-PIBUT] range varying from 0 to 1%, stress-strain curves show a stress peak at small strain, followed by a plateau in stress and a sharp decrease from $\sigma_0 \approx 10^5$ Pa to $\sigma_0 \leq 10^4$ Pa. The critical stretching ratio $\lambda_{0,c}$ measured when a sharp drop of stress is observed, decreases when [M-PIBUT] increases. Beyond $\lambda_{0,c}$, the decrease in nominal stress in this final step is more pronounced when the concentration of multifunctional polymers increases. For [M-PIBUT] = 5%, no stress plateau is observed and the stress-strain curve is reduced to a high stress peak.

Similar trends are observed at low debonding speed (V_{deb}=1 µm/s), except that no discontinuous drop of stress is observed at large strain for PIBUT and Blend_0.1.

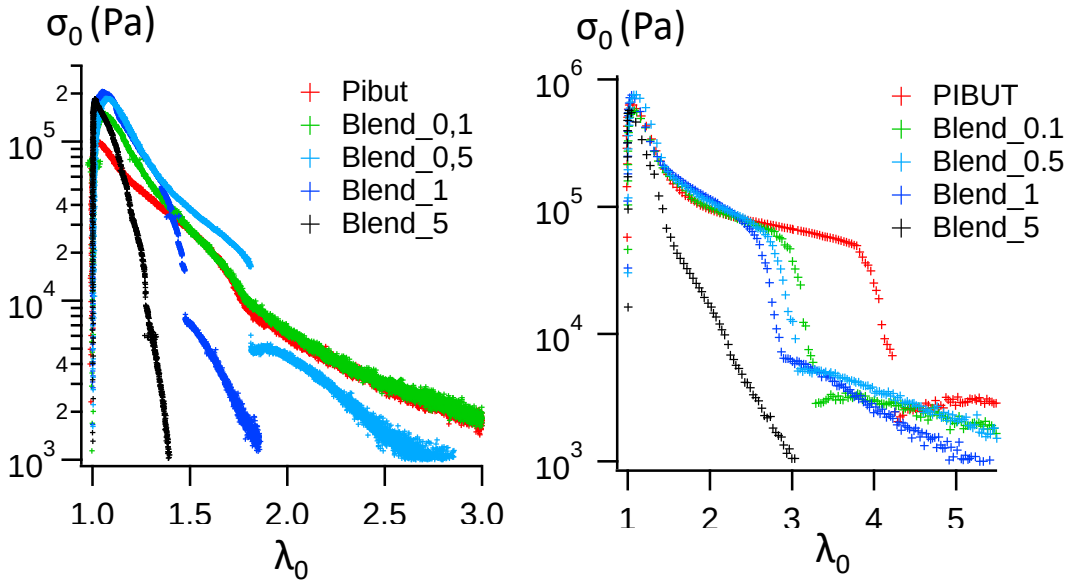

Figure 8: probe-tack curves at 1 (left) and 100µm/s (right)

The shape of the stress-strain curve, observed at 100µm/s over the [M-PIBUT] range from 0 to 1% and at 1µm/s for [M-PIBUT]=0.5 and 1%, is characteristic of confined viscous or viscoelastic films[21,19], i.e. when the contact radius r_0 is much larger than the initial thickness h_0 (r_0/h_0=30 in our case). The variation of σ_0 with λ_0 is closely linked to the flow of the adhesive as well as the nucleation and macroscopic growth of internal bubbles and Saffman-Taylor fingers during the probe-tack test, as illustrated by the debonding patterns in figure 9 and S8. Clearly the different materials tested form very different patterns as the probe is pulled.

The low compliance of the confined adhesive layer induces high stress at the beginning of the debonding step[19] and the first drop in force is caused by the cavitation process. As cavities grow from the probe surface into the film, stress relaxes through the film and the spring-like response of the apparatus induces a large deformation of the adhesive layer[30,31,32]. The break-up of the walls between cavities and the Saffman-Taylor instabilities growing from the external periphery induce the equilibration of the pressure[19,15] between the ambient atmosphere and the internal cavities and thus, a rapid drop of stress. After this step, the measured stresses result from the elongation of the remaining fibrils between the probe and the adhesive layer and are characteristic of a cohesive failure (see figures S8-S9).

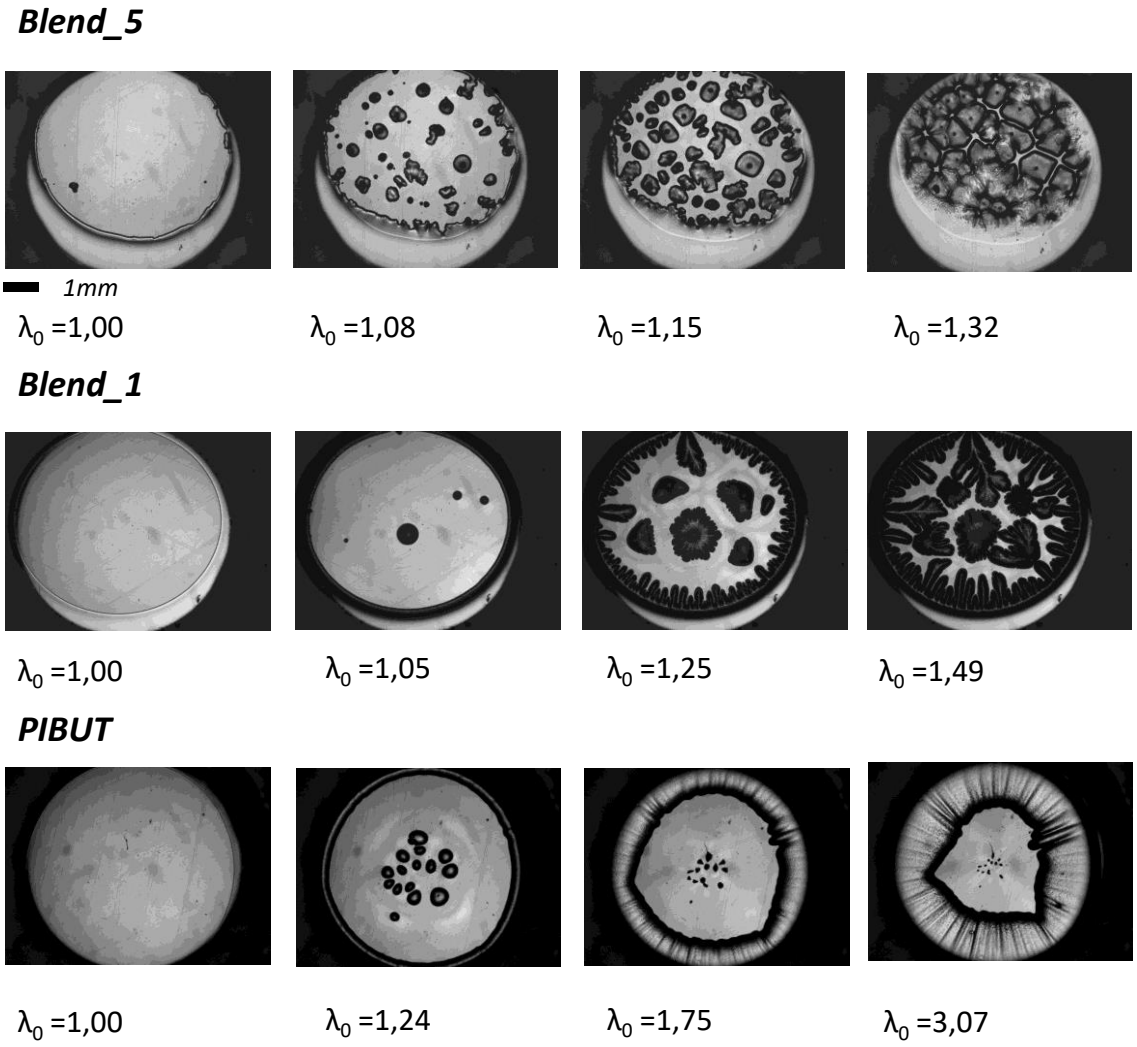

Figure 9: debonding patterns at 1 µm/s for pure PIBUT, Blend_1 and Blend_5.

In the cases of the probe-tack tests carried out on PIBUT and Blend_0.1 at 1µm/s, the absence of a drastic decrease in stress is characteristic of low viscosity liquids or low debonding speeds[31]. Although bubbles initially grow into the adhesive layer, their size eventually decreases in a drastic way as the adhesive layer is stretched and the pressure reequilibrates, as observed in figure 9. No coalescence of cavities with the external periphery occurs and thus, no sharp stress reduction is detected. On the opposite direction, the stress-

strain curve of Blend_5, which is limited to a stress peak, reveals the behavior of soft elastic layers[26,22,33]. As observed in figures S8-S9, little or no residue is left on the probe after the test.

The adhesion energy, measured by the area of the stress-strain curves is displayed in table 4 for both debonding velocities. At low concentrations ([M-PIBUT]<1%), rather similar adhesion energy W_{adh} is observed for all samples (W_{adh} ≈ 40J/m^2 at 100µm/s and W_{adh} ≈ 5J/m^2 at 1µm/s). At higher [M-PIBUT], the debonding energy is strongly reduced (W_{adh} ≈ 10J/m^2 at 100µm/s and W_{adh} ≈ 3J/m^2 at 1µm/s).

	E_{adh} (J/m^2) (100µm/s)	E_{adh} (J/m^2) (1µm/s)
PIBUT	41 ± 4	3.8 ± 1
Blend_0.1	36 ± 4	5.3± 1
Blend_0.5	42 ± 4	6.4± 1
Blend_1	41 ± 4	5.7 ± 1
Blend_5	13 ± 2	2.5 ± 0.5

Table 4: Adhesion energy measured for PIBUT/M-PIBUT blends

Discussion

Multifunctional Chains as Supramolecular Cross-linkers

The study of the linear rheology below and above the order/disorder transition temperature (80°C≥T_{ODT} ≥60°C for PIBUT[10]) sheds light on the effect of multifunctional chains on the dynamics of supramolecular associations and on the mobility of the aggregates. At 80°C, the liquid state of the supramolecular blends suggests that the rheological behavior is investigated above T_{ODT} and characterizes the flow of the supramolecular filaments[34], the relaxation processes of which, are governed by the dynamics of stickers. The non Newtonian behavior observed at low frequency may be due to the presence of long time relaxing but diluted aggregates[29]. Adding multifunctional chains modifies little the rheological behavior at high temperature (see figures 5 and S6). This liquid state contrasts with the solid behavior of M-PIBUT (without adding extra PIBUT) at 80°C. The low viscoelastic moduli measured at high temperature suggest that PIBUT plays the role of solvent for M-PIBUT. The bis-urea moiety of PIBUT interacts with the moieties of multifunctional chains preventing the formation of a supramolecular network and thus, induces the flow of supramolecular chains.

As T decreases below T_{ODT}, the effect of multifunctional chains becomes clearly visible. During the temperature ramp, the sol-gel transition appears faster (i.e. at a higher temperature) with increasing concentration of M-PIBUT (see figure 5). After annealing the sample for 24 hours at 25°C, the supramolecular blends are more elastic at high [M-PIBUT] (see figure 6) and in large deformations, the resistance to creep is also improved when PIBUT is blended with M-PIBUT. These results stem from the reduction in mobility of the supramolecular aggregates induced by the multifunctional chains. In agreement with the SAXS data, the rheology of supramolecular blends reinforces the assumption that the bis-urea moieties of M-PIBUT are indeed incorporated into the rod-like aggregates and act as bridges between filaments. At high concentration of M-PIBUT, the mobility of the rods-like aggregates at the sol/gel transition would be too low to allow a long range molecular organization. The disruption of the nanostructure at a micrometric scale observed in blends in AFM and SAXS would be due to a kinetic effect linked to these physical cross-links (see figures 3-4).

Effects of Multifunctional Chains on the adhesion tests

In the field of soft adhesives, chemical and/or physical cross-linking is a well-known process to optimize the peel force or tackiness of thin polymer layers via a modification of their rheological properties. The transition from viscoelastic liquid to soft solid induced by increasing the degree of cross-linking goes along with a transition in failure mechanism (from cohesive to adhesive). In the present study, the effect of multifunctional chains on the adhesive properties of soft nanostructured materials was investigated by varying their concentration in these systems. As previously discussed, preliminary rheological and structural characterizations highlighted the role of these multivalent chains as supramolecular cross-linkers. A transition from a cohesive to an adhesive debonding mode occurred as expected at a critical density of M-PIBUT (between 1 and 5%), as illustrated by the images of the steel probe after tests (see figures S8-S9).

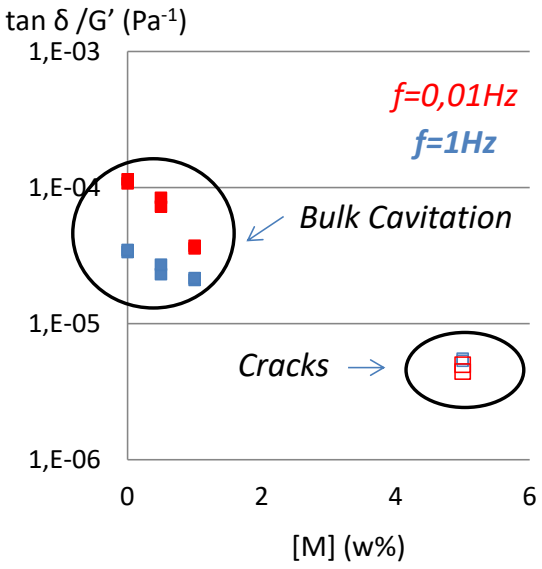

Figure 10: Variation of tan(δ)/G' measured at two frequencies f=1Hz (*blue*) and f=0.01Hz (*red*) with the concentration of M-PIBUT for the supramolecular blends. Filled and unfilled markers represent the cohesive and adhesive, respectively, mode of fracture observed during the probe-tack test at the equivalent frequency $f=V_{deb}/h_0$.

At low concentrations of M-PIBUT (≤1%), the cohesive mode of failure and the debonding mechanisms observed during the probe-tack tests, such as cavitation and fibrillation processes, are typical of viscoelastic fluids in a confined state[19]. At high concentrations of M-PIBUT (≥5%), the adhesive mode of fracture resulting from the fast propagation of interfacial cracks are characteristic of elastic and weakly dissipative materials[26,22]. The change of debonding mode occurring between 1 and 5% of M-PIBUT results from the elasticity[23,18] of the supramolecular blends, which is more and more pronounced with increasing [M-PIBUT]. As proposed by Deplace and coworkers[17], the relationship between linear rheology and mode of failure can be illustrated here with the *tanδ/G'* ratio measured at the equivalent frequency $f=V_{deb}/h_0$, as shown in figure 10. As observed in previous studies, below a critical *tanδ/G'* ratio, the elastic energy stored in the thin layer is transferred to the contact lines of cavities and cracks can propagate at the interface between the probe and the thin adhesive without significant deformation of the adhesive[23,18].

The similarities between chemical crosslinking and supramolecular crosslinking stops however there. In numerous studies[35] published in the literature, the transition from liquid-like to solid-like behavior induced by a *chemical covalent* cross-linking process goes along with a *maximum* of the debonding energy. In the probe-tack test, this maximum results from the large deformations of fibrils before breaking or detaching from the probe. Although PIBUT flows at large deformations like any viscous liquids, the strengthening effect of M-PIBUT on PIBUT gives the opposite effect. A shown in figure 8, at low concentration of M-PIBUT (≤1%), the variation of the shape of the stress-strain curves relative to pure PIBUT suggests that fibrils are less stable under stress with increasing [M-PIBUT]: the coalescence

of bubbles occurs at smaller deformations and the residual stress after the equilibration of pressure declines faster. Moreover the change of debonding mode (observed for Blend_5) is characterized by a drop of the debonding energy and does not show any cavitation and fibrillation processes.

Propagation of Cavities

In order to shed more light on the link between the rheology of the supramolecular blends and their deformations in the probe-tack tests, the deformation of the adhesive layer visualized through the camera was quantitatively characterized with the image analysis tools developed by Tanguy and coworkers[15].

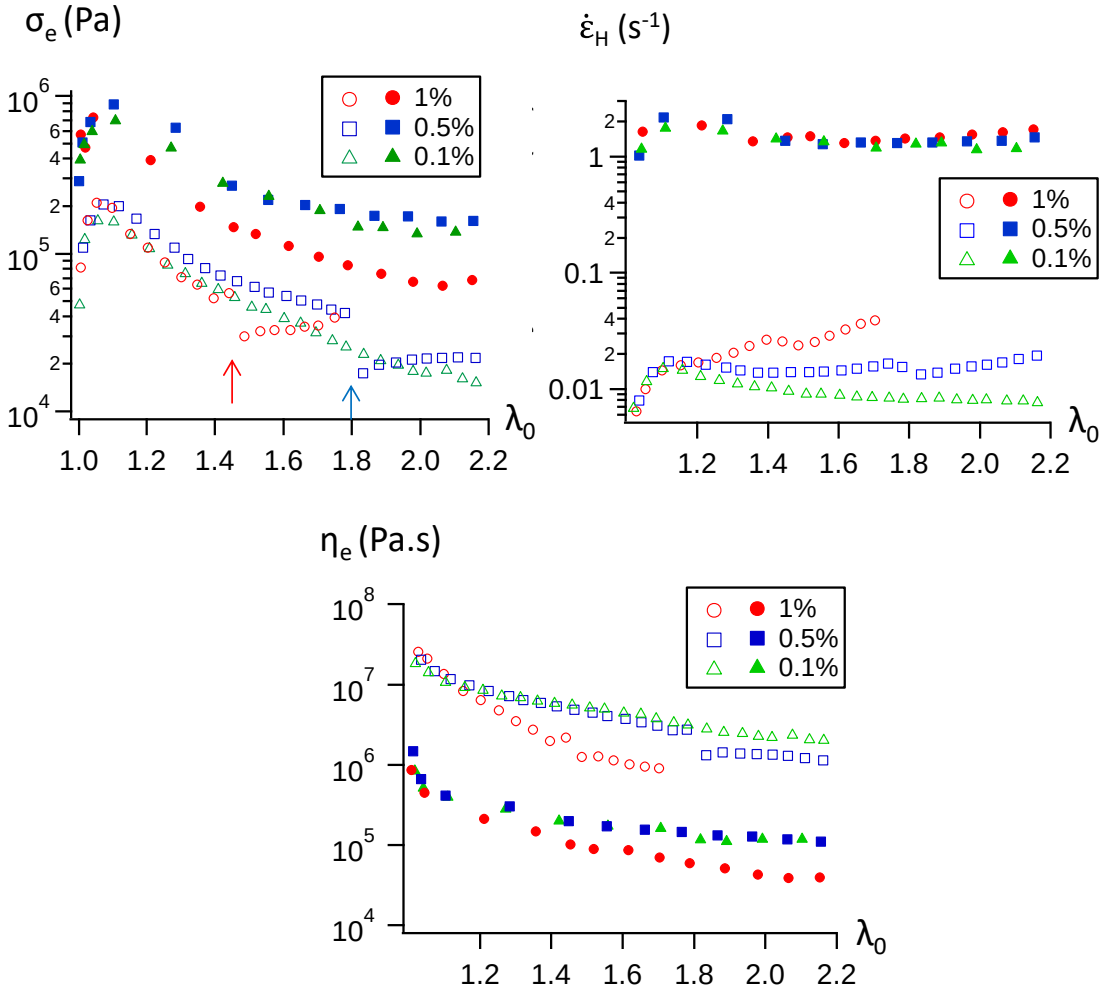

Figure 11: The dependence of the normal component σ_e of stresses in fibrils, the local Hencky strain rate $\dot{\varepsilon}_H$ and the local elongation viscosity η^+ on the nominal elongation rate λ_0 for adhesion tests carried out at 1µm/s (unfilled markers) and 100µm/s (filled markers) on Blend_0.1, Blend_0.5 and Blend_1.

For low concentrations of M-PIBUT (≤1%), a fibrillar structure is formed during the debonding process and walls are stretched between bubbles until the complete detachment of the steel probe from the adhesive layer. In this case, the analysis of the debonding images

synchronized with the force sensor can be used to estimate the normal component σ_e of stresses in fibrils, a local Hencky strain rate $\dot{\varepsilon_H}$ and a local elongation viscosity η^+ from the projected area of cavities and that of fibrils (see the experimental section). The variation of these three parameters with the nominal elongation rate λ_0 is shown in figure 11 for adhesion tests carried out at 1µm/s and 100µm/s. For V_{deb}=1µm/s, the parameters $\dot{\varepsilon_H}$, σ_e and η^+ are measured before and after the equilibration of pressure while for V_{deb}=100µm/s, they were only estimated before the coalescence of cavities due to experimental noise. The equilibration of pressure is noticed by an arrow.

In figure 11, the variation of the effective stress σ_e and that of the local extensional viscosity η^+ with the nominal strain λ_0 enhance the flow rate of the polymer chains in the fibrils. For the three blends and both debonding velocities, σ_e and η^+ slightly decrease after the cavitation process ($\lambda_0 \geq 1{,}1$) and are roughly constant at large deformations. While no clear strengthening of fibrils from M-PIBUT is observed through the measures of σ_e and η^+, a significant effect of M-PIBUT on the local Hencky strain rate $\dot{\varepsilon_H}$ can be noticed.

As expected, $\dot{\varepsilon}_H$ is of the same order of magnitude that the equivalent strain rate $\dot{\varepsilon}_{eq}=V_{deb}/h_0$: $\dot{\varepsilon}_{eq}\approx 1s^{-1}$ for $V_{deb}=100\mu m/s$ and $\dot{\varepsilon}_{eq}\approx 0{,}01s^{-1}$ for $V_{deb}=1\mu m/s$. At low V_{deb}, different trends are clearly observed between the three blends. At 0,5% and 1% of M-PIBUT, $\dot{\varepsilon_H}$ increases with the nominal strain while $\dot{\varepsilon_H}$ continuously decreases with λ_0 at 0,1% of M-PIBUT. At a fixed λ_0, $\dot{\varepsilon}_H$ increases with the concentration of multifunctional chains. The effect of the multifunctional chains is less pronounced at higher debonding velocities. For V_{deb}=100µm/s, $\dot{\varepsilon}_H$ is quite similar for all blends and a slight increase $\dot{\varepsilon}_H$ with [M-PIBUT] is only perceived at high λ_0.

The local Hencky strain rate $\dot{\varepsilon}_H$ is measured from the variation of the projected area of fibrils and thus, characterizes the growth of cavities and the thinning mechanisms of fibrils. Since $\dot{\varepsilon}_H$ increases with [M-PIBUT] at a fixed nominal deformation λ_0, cavities grow faster and fibrils become rapidly thinner with increasing [M-PIBUT]. These mechanisms reveal that fibrils localize more the strain and are *less stable under stress* with increasing [M-PIBUT]. Such strain localization mechanism was recently observed for soft nanostructured materials composed of tri-urea center-functionalized poly(butylacrylate)[24] but was assumed to be the consequence of the strain softening of the supramolecular structure at large deformations[24]. In this previous study, however, there were no bridging supramolecular chains. In a more microscopic way, as the cavities nucleate and grow into the thin adhesive layer, the nanostructured material softens at the edges of the cavities, where local stresses are higher. This local softening mechanism accelerates the propagation of cavities until the rupture of the walls.

In the present case, it is worth noting that the strain localization mechanism is particularly pronounced for V_{deb}=1µm/s while such process is less discernable for V_{deb}=100µm/s. Likewise, a strong influence of [M-PIBUT] on $\dot{\varepsilon}_H$ is observed at low debonding velocity while the variation of $\dot{\varepsilon_H}$ is similar for the three investigated blends at high debonding velocity. A

similar discrepancy between short and long time scales is observed for the strain sweeps carried out in the rheometer at both equivalent angular frequencies $\omega=2\pi V_{deb}/h_0$: $\omega_1=2\pi.10^{-2}$ rad/s and $\omega_2=2\pi$ rad/s. The resistance to flow is clearly improved with increasing [M-PIBUT] for $\omega=\omega_1$ while similar responses are observed for the three materials for $\omega=\omega_2$.

If we assume that the strengthening effect of M-PIBUT is qualitatively the same in shear experiments than in extensional tests, the comparison between non-linear rheology in shear and fibril stability in adhesion is important and suggests that the mechanism of strain localization observed in the adhesive tests is enhanced by a higher resistance to flow at large strain, which is counter-intuitive. Again let's try a microscopic view: if the elongation of fibrils between cavities requires higher stresses, local stresses around cavities are also higher and the local strain softening is more pronounced. The enhancement of this local softening mechanism would make the cavities propagate faster until the rupture of the walls. This counter-intuitive result suggests that strong strain hardening mechanisms are required to get a good stability of bubbles while fibrils are stretched. Increasing the resistance to creep (a small strain effect) is clearly not sufficient to get large bulk deformation in adhesion tests and, as shown in previous studies[17], the design of soft adhesives requires a precise equilibrium between softening at intermediate strains and hardening at larger strains.

The comparison between low and high frequencies in rheology and adhesion also sheds light on some key molecular features for the design of supramolecular adhesives. At low frequency, rheology is governed by the dynamics of supramolecular rod-like aggregates[29], which are formed by the self-assembly of bis-urea moieties. At high frequency, rheology is also affected by the relaxation of the side chains[29]. For $\omega_1=2\pi.10^{-2}$ rad/s, the acceleration of the thinning process of fibrils with increasing [M-PIBUT] reveals that reducing the mobility of the aggregates favors the strain localization mechanism and thus, low debonding energies. On the opposite, the large deformations of fibrils observed for $\omega_2=2\pi$ rad/s suggest that the local friction between aggregates via the side chains favors the stability of cavities and thus, high debonding energies. High mobility of the self-assembled structures, which would favor *fast recombination after scission* under stress, and large energy dissipation through the surrounding polymer matrix are two key-points to design soft nanostructured materials with high adhesive properties.

From the two previous paragraphs, one can conclude that physically cross-linking supramolecular aggregates is *not equivalent* to chemically cross-linking the polymer chains bearing multiple interacting moieties[35]. Contrary to chemically cross-linked chains, short multifunctional chains need the supramolecular nanostructure to be effective. Hence multifunctional chains reinforce the elasticity of the nanostructured in small strain and increase its resistance to creep. However, beyond the yield stress these physical cross-linkers cannot prevent the material from flowing and the nanostructure does not reform fast enough in large strain to provide the strain hardening needed for clean detachment. This suggests that for applications where both dissipative and strain hardening properties are

required, the nanostructure must be either able to withstand nearly reversible deformations to large strains (like thermoplastic elastomer systems such as styrene-isoprene-styrene triblock copolymers[36]), or the nanostructure must be relatively dynamic to reform quickly under large strains.

Conclusion

The nanostructure, non-linear and linear rheology and the adhesive properties of supramolecular materials elaborated by blending monofunctional and multifunctional poly(isobutene) (PIB) chains were investigated in the melt state. Monofunctional PIB (PIBUT) are linear and unentangled polymer chains (M_n≈3kg/mol) functionalized in the middle by a bis-urea interacting moiety, able to self-associate by four hydrogen bonds. Multifunctional chains (M-PIBUT) bearing two or three such bis-urea stickers were also synthesized and mixed with PIBUT. The characterization of the supramolecular blends by SAXS and AFM revealed that multifunctional and monofunctional chains interact with each other to form bundles of rod-like aggregates but the incorporation of small amounts of M-PIBUT significantly disrupts the long range order of the structure. However, despite this decrease in order, non-linear rheology shows a strengthening with increasing concentration of M-PIBUT and suggests that M-PIBUT physically cross-links the supramolecular filaments.

The most interesting result is that although a transition from liquid-like to solid behavior is observed in probe-tack tests at 5% of M-PIBUT, no significant improvement of the adhesive properties is obtained with increasing the concentration of multifunctional chains. The debonding mechanisms change directly from a fibrillar cohesive mode to an interfacial adhesive mode and no fibrillar and adhesive debonding mode is observed. This result is due to the fact that adding M-PIBUT decreases strongly viscoelastic dissipation in small strain and increases weakly the strain hardening in large strain. This last feature is due to the fact that once this nanostructure fails in large strain, it is not able to reform and to provide a strain hardening mechanism. As a result, failure in the supramolecular blends induces a strong strain localization mechanism during the adhesion and thus, low debonding energies. For future applications of supramolecular chemistry in adhesives it will be crucial to finely tune both small-strain viscoelasticity and large strain hardening.

References

(1) Heinzmann, C.; Weder, C.; de Espinosa, L. M. Supramolecular Polymer Adhesives: Advanced Materials Inspired by Nature. *Chem Soc Rev* **2016**, *45* (2), 342–358 DOI: 10.1039/C5CS00477B.

(2) Aida, T.; Meijer, E. W.; Stupp, S. I. Functional Supramolecular Polymers. *Science* **2012**, *335* (6070), 813–817 DOI: 10.1126/science.1205962.

(3) Goldansaz, H.; Fustin, C.-A.; Wübbenhorst, M.; van Ruymbeke, E. How Supramolecular Assemblies Control Dynamics of Associative Polymers: Toward a General Picture. *Macromolecules* **2016**, *49* (5), 1890–1902 DOI: 10.1021/acs.macromol.5b01535.
(4) Chen, S.; Döhler, D.; Binder, W. H. Rheology of Hydrogen-Bonded Dendritic Supramolecular Polymer Networks in the Melt State. *Polymer* **2016**, *107*, 466–473 DOI: 10.1016/j.polymer.2016.08.046.
(5) Yan, T.; Schröter, K.; Herbst, F.; Binder, W. H.; Thurn-Albrecht, T. What Controls the Structure and the Linear and Nonlinear Rheological Properties of Dense, Dynamic Supramolecular Polymer Networks? *Macromolecules* **2017**, *50* (7), 2973–2985 DOI: 10.1021/acs.macromol.6b02507.
(6) Yan, T.; Schröter, K.; Herbst, F.; Binder, W. H.; Thurn-Albrecht, T. Unveiling the Molecular Mechanism of Self-Healing in a Telechelic, Supramolecular Polymer Network. *Sci. Rep.* **2016**, *6* (1) DOI: 10.1038/srep32356.
(7) Herbst, F.; Schröter, K.; Gunkel, I.; Gröger, S.; Thurn-Albrecht, T.; Balbach, J.; Binder, W. H. Aggregation and Chain Dynamics in Supramolecular Polymers by Dynamic Rheology: Cluster Formation and Self-Aggregation. *Macromolecules* **2010**, *43* (23), 10006–10016 DOI: 10.1021/ma101962y.
(8) Croisier, E.; Liang, S.; Schweizer, T.; Balog, S.; Mionić, M.; Snellings, R.; Cugnoni, J.; Michaud, V.; Frauenrath, H. A Toolbox of Oligopeptide-Modified Polymers for Tailored Elastomers. *Nat. Commun.* **2014**, *5* (4728) DOI: 10.1038/ncomms5728.
(9) Pensec, S.; Nouvel, N.; Guilleman, A.; Creton, C.; Boué, F.; Bouteiller, L. Self-Assembly in Solution of a Reversible Comb-Shaped Supramolecular Polymer. *Macromolecules* **2010**, *43* (5), 2529–2534 DOI: 10.1021/ma901709e.
(10) Courtois, J.; Baroudi, I.; Nouvel, N.; Degrandi, E.; Pensec, S.; Ducouret, G.; Chanéac, C.; Bouteiller, L.; Creton, C. Supramolecular Soft Adhesive Materials. *Adv. Funct. Mater.* **2010**, *20* (11), 1803–1811 DOI: 10.1002/adfm.200901903.
(11) Creton, C. Pressure-Sensitive-Adhesives : An Introductory Course. *MRS Bull.* **2003**, *28* (6), 434–439.
(12) Way, A. E.; Korpusik, A. B.; Dorsey, T. B.; Buerkle, L. E.; von Recum, H. A.; Rowan, S. J. Enhancing the Mechanical Properties of Guanosine-Based Supramolecular Hydrogels with Guanosine-Containing Polymers. *Macromolecules* **2014**, *47* (5), 1810–1818 DOI: 10.1021/ma402618z.
(13) Koenigs, M. M. E.; Pal, A.; Mortazavi, H.; Pawar, G. M.; Storm, C.; Sijbesma, R. P. Tuning Cross-Link Density in a Physical Hydrogel by Supramolecular Self-Sorting. *Macromolecules* **2014**, *47* (8), 2712–2717 DOI: 10.1021/ma500446g.
(14) Tharcis, M.; Breiner, T.; Belleney, J.; Boué, F.; Bouteiller, L. Hydrogen Bonded Supramolecular Polymers in Protic Solvents: Role of Multitopicity. *Polym. Chem.* **2012**, *3* (11), 3093–3099 DOI: 10.1039/C2PY20287E.
(15) Tanguy, F.; Nicoli, M.; Lindner, A.; Creton, C. Quantitative Analysis of the Debonding Structure of Soft Adhesives. *Eur. Phys. J. E* **2014**, *37* (1), 1–12.
(16) Derail, C.; Allal, A.; Marin, G.; Tordjeman, P. Relationship between Viscoelastic and Peeling Properties of Model Adhesives. Part 1. Cohesive Fracture. *J. Adhes.* **1997**, *61* (1–4), 123–157 DOI: 10.1080/00218469708010519.
(17) Deplace, F.; Carelli, C.; Mariot, S.; Retsos, H.; Chateauminois, A.; Ouzineb, K.; Creton, C. Fine Tuning the Adhesive Properties of a Soft Nanostructured Adhesive with Rheological Measurements. *J. Adhes.* **2009**, *85* (1), 18–54 DOI: 10.1080/00218460902727381.

(18) Creton, C.; Ciccotti, M. Fracture and Adhesion of Soft Materials: A Review. *Rep. Prog. Phys. Phys. Soc. G. B.* **2016**, *79* (4), 046601 DOI: 10.1088/0034-4885/79/4/046601.
(19) Poivet, S.; Nallet, F.; Gay, C.; Teisseire, J.; Fabre, P. Force Response of a Viscous Liquid in a Probe-Tack Geometry: Fingering versus Cavitation. *Eur. Phys. J. E* **2004**, *15* (2), 97–116 DOI: 10.1140/epje/i2004-10040-2.
(20) Derks, D.; Lindner, A.; Creton, C.; Bonn, D. Cohesive Failure of Thin Layers of Soft Model Adhesives under Tension. *J. Appl. Phys.* **2003**, *93* (3), 1557–1566 DOI: 10.1063/1.1533095.
(21) Lakrout, H.; Creton, C.; Ahn, D.; Shull, K. R. Influence of Molecular Features on the Tackiness of Acrylic Polymer Melts. *Macromolecules* **2001**, *34* (21), 7448–7458 DOI: 10.1021/ma0020279.
(22) Nase, J.; Lindner, A.; Creton, C. Pattern Formation during Deformation of a Confined Viscoelastic Layer: From a Viscous Liquid to a Soft Elastic Solid. *Phys. Rev. Lett.* **2008**, *101* (7) DOI: 10.1103/PhysRevLett.101.074503.
(23) Crosby, A. J.; Shull, K. R.; Lakrout, H.; Creton, C. Deformation and Failure Modes of Adhesively Bonded Elastic Layers. *J. Appl. Phys.* **2000**, *88* (5), 2956–2966 DOI: 10.1063/1.1288017.
(24) Callies, X.; Fonteneau, C.; Pensec, S.; Bouteiller, L.; Ducouret, G.; Creton, C. Adhesion and Non-Linear Rheology of Supramolecular Tri-Urea Center-Functionalized Poly(Butylacrylate) Investigated by Probe-Tack Tests. *Soft Matter* **2016**, *12*, 7174–7185.
(25) Binder, W. H.; Machl, D. Poly(Ether Ketone)–polyisobutylene Block Copolymers: Synthesis and Phase Behavior. *J. Polym. Sci. Part Polym. Chem.* **2005**, *43* (1), 188–202 DOI: 10.1002/pola.20483.
(26) Josse, G.; Sergot, P.; Creton, C.; Dorget, M. MEASURING INTERFACIAL ADHESION BETWEEN A SOFT VISCOELASTIC LAYER AND A RIGID SURFACE USING A PROBE METHOD. *J. Adhes.* **2004**, *80* (1–2), 87–118 DOI: 10.1080/00218460490276821.
(27) Zosel, A. Adhesion and Tack of Polymers: Influence of Mechanical Properties and Surface Tensions. *Colloid Polym. Sci.* **1985**, *263* (7), 541–553.
(28) Véchambre, C.; Callies, X.; Fonteneau, C.; Ducouret, G.; Pensec, S.; Bouteiller, L.; Creton, C.; Chenal, J.-M.; Chazeau, L. Microstructure and Self-Assembly of Supramolecular Polymers Center-Functionalized with Strong Stickers. *Macromolecules* **2015**, *48* (22), 8232–8239 DOI: 10.1021/acs.macromol.5b01584.
(29) Callies, X.; Véchambre, C.; Fonteneau, C.; Pensec, S.; Chenal, J.-M.; Chazeau, L.; Bouteiller, L.; Ducouret, G.; Creton, C. Linear Rheology of Supramolecular Polymers Center-Functionalized with Strong Stickers. *Macromolecules* **2015**, *48* (19), 7320–7326 DOI: 10.1021/acs.macromol.5b01583.
(30) Francis, B. A.; Horn, R. G. Apparatus-Specific Analysis of Fluid Adhesion Measurements. *J. Appl. Phys.* **2001**, *89* (7), 4167–4174 DOI: 10.1063/1.1351057.
(31) Poivet, S.; Nallet, F.; Gay, C.; Fabre, P. Cavitation-Induced Force Transition in Confined Viscous Liquids under Traction. *EPL Europhys. Lett.* **2003**, *62* (2), 244–250.
(32) Tirumkudulu, M.; Russel, W. B.; Huang, T. J. On the Measurement of "Tack" for Adhesives. *Phys. Fluids* **2003**, *15* (6), 1588–1605 DOI: 10.1063/1.1571058.
(33) Nase, J.; Creton, C.; Ramos, O.; Sonnenberg, L.; Yamaguchi, T.; Lindner, A. Measurement of the Receding Contact Angle at the Interface between a Viscoelastic Material and a Rigid Surface. *Soft Matter* **2010**, *6* (12), 2685 DOI: 10.1039/c001687j.

(34) Callies, X.; Fonteneau, C.; Véchambre, C.; Pensec, S.; Chenal, J.-M.; Chazeau, L.; Bouteiller, L.; Ducouret, G.; Creton, C. Linear Rheology of Bis-Urea Functionalized Supramolecular Poly(Butylacrylate)s: Part I – Weak Stickers. *Polymer* **2015**, *69*, 233–240 DOI: 10.1016/j.polymer.2014.12.053.
(35) Callies, X.; Herscher, O.; Fonteneau, C.; Robert, A.; Pensec, S.; Bouteiller, L.; Ducouret, G.; Creton, C. Combined Effect of Chain Extension and Supramolecular Interactions on Rheological and Adhesive Properties of Acrylic Pressure-Sensitive Adhesives. *ACS Appl. Mater. Interfaces* **2016**, *8* (48), 33307–33315 DOI: 10.1021/acsami.6b11045.
(36) Creton, C.; Hu, G.; Deplace, F.; Morgret, L.; Shull, K. R. Large-Strain Mechanical Behavior of Model Block Copolymer Adhesives. *Macromolecules* **2009**, *42* (20), 7605–7615 DOI: 10.1021/ma900821k.